WATER RESOURCES RESEARCH, VOL. 49, 1611–1624, doi:10.1002/wrcr.20140, 2013

Influence of spatial temperature estimation method in ecohydrologic modeling in the Western Oregon Cascades

Elizabeth S. Garcia,[1] Christina L. Tague,[2] and Janet S. Choate[2]

Received 4 May 2012; revised 28 January 2013; accepted 8 February 2013; published 28 March 2013.

[1] Most spatially explicit hydrologic models require estimates of air temperature patterns. For these models, empirical relationships between elevation and air temperature are frequently used to upscale point measurements or downscale regional and global climate model estimates of air temperature. Mountainous environments are particularly sensitive to air temperature estimates as spatial gradients are substantial, and air temperature plays a critical role in snow-related processes. We use a distributed, coupled ecohydrologic model to compare estimates of streamflow, snowmelt, transpiration, and net primary productivity (NPP) using five temperature interpolation approaches for a forested mountain basin that is dominated by a rain-snow zone in Western Oregon, USA. We compare model estimates using a standard adiabatic lapse rate of $-6.5°\mathrm{C\ km^{-1}}$; basin-specific lapse rates created using daily point observations at high, middle, and low elevations; and gridded temperature estimates from the Parameter-elevation Regressions on Independent Slopes Model (PRISM) derived at 800 and 50 m resolutions. We show that temperature interpolation strategies influence model calibration. Point-based estimates using a low-elevation station or 800 m PRISM grids result in significantly fewer parameter sets that model streamflow well, suggesting a bias in parameter selection due to errors in input data. The greatest postcalibration impact of temperature lapse rate estimates occurs for model estimates of NPP. The constant temperature lapse rate results in substantially reduced NPP estimates that are more sensitive to the interannual variation in climate forcing.

Citation: Garcia, E. S., C. L. Tague, and J. S. Choate (2013), Influence of spatial temperature estimation method in ecohydrologic modeling in the Western Oregon Cascades, *Water Resour. Res.*, *49*, 1611–1624, doi:10.1002/wrcr.20140.

1. Introduction

[2] Spatial and temporal variation in climate forcing is difficult to capture in mountainous terrain due to the high spatial heterogeneity coupled with sparse meteorologic instrumentation [*Running et al*., 1987; *Chen et al*., 1999; *Minder et al*., 2010]. Commonly used interpolation approaches may lead to substantial interpolation bias in these regions, particularly because climate stations are often located at relatively low elevations [*Phillips et al*., 1992]. Temperature interpolation can also be confounded in locations susceptible to cold-air pooling, which occurs when cold, dense air collects in a mountain valley and becomes stagnant, leading to atmospheric decoupling from air at higher elevations [*Whiteman*, 2000]. In regions susceptible to atmospheric decoupling, typical temperature interpolation techniques do not accurately reflect the regional air temperature pattern [*Lundquist*, 2008]. Distributed hydrologic and coupled ecohydrologic models typically require continuous spatial coverage of meteorologic input data; however, errors in interpolated temperature are a large source of uncertainty in distributed modeling [*Chen et al*., 1999; *Liston and Elder*, 2006]. Inaccurate representation of spatial patterns may have important implications for developing climate change scenarios and for improving our understanding of modeling the synergistic interactions between environmental change and ecohydrologic processes [*Baron et al*., 1998; *Gerten et al*., 2004; *Luo et al*., 2008]. When the source of input data is station data, measurements must be interpolated over space. In climate change scenario development, ecologic and hydrologic models are driven by regional and global climate model outputs. The spatial resolution of global and regional climate model estimates remains relatively coarse [*Huffman et al*., 2001; *Hack et al*., 2006; *Pierce et al*., 2009], and meteorologic inputs derived from climate models must typically be downscaled to capture local patterns, especially in mountain environments.

[3] For both upscaling of point and downscaling of gridded inputs, a $-6.5°\mathrm{C\ km^{-1}}$ lapse rate with elevation is often applied to approximate temperature patterns. This value represents the mean environmental lapse rate of stationary air with an average moisture content [*Ahrens*, 2007] and does not reflect the seasonal variation of a region

[1]Department of Geography, University of California at Santa Barbara, Santa Barbara, California, USA.
[2]Bren School of Environmental Management, University of California at Santa Barbara, Santa Barbara, California, USA.

Corresponding author: E. S. Garcia, Department of Geography, University of California, Santa Barbara, CA 93106-5131, USA. (garcia@geog.ucsb.edu)

0043-1397/13/10.1002/wrcr.20140

susceptible to atmospheric decoupling and cold-air pooling. Additionally, it does not account for the topographic influence of hillslope angle and aspect [*Barry*, 1992]. Optimally, data recorded by a dense network of sensors would be used to characterize spatial and temporal patterns of surface temperature [*Lookingbill and Urban*, 2003; *Lundquist and Cayan*, 2007]. However, as resources are seldom available to implement such projects, approximations are improved by empirical relationships with topography that are derived from local data and allow the temperature lapse rate to vary seasonally. Using local station observations to create a region-specific constant lapse rate improves the accuracy of estimated air temperature surfaces [*Dodson and Marks*, 1997; *Jarvis and Stuart*, 2001] as does using more sophisticated statistical methods such as the Parameter-elevation Regressions on Independent Slopes Model (PRISM) [*Daly et al*., 1994, 2002, 2008], which accounts for prevailing storm directions, proximity to the ocean, seasonal temperature inversions, cold-air drainage and pooling, and other landscape controls on temperature patterns. While these approaches generally estimate temperature better than a mean adiabatic lapse rate (MALR), all must make simplified assumptions in order to make estimates in areas of rugged terrain spanning a wide range of elevations.

[4] In the mountains of the western United States, accurate representation of temperature patterns is particularly important in the rain-snow transition zone. Temperature is a key control on partitioning incoming precipitation between rain and snow [*U.S. Army Corps of Engineers*, 1956; *Nolin and Daly*, 2006] and influences when and where snowmelt occurs. *Lundquist et al*. [2008a, 2008b] show that in the California American River Basin, a 100 m location error in the snow-rain transition zone is approximately equivalent to a 5% error in contributing runoff area during a storm. Changes in the amount and timing of snowmelt translate into changes in the seasonal timing of streamflow [*Cayan et al*., 2001; *Stewart et al*., 2004; *Hamlet et al*., 2005; *Bales et al*., 2006]. In mountain environments, temperature patterns and associated snow dynamics are also key controls on ecologic processes and influence plant phenology [*Schwartz*, 1994; *Schwartz and Reiter*, 2000; *Parmesan*, 2007], plant water use [*Tague and Dugger*, 2010], and net primary productivity (NPP) [*Stephenson and Mantgem*, 2005; *Boisvenue and Running*, 2006]. These prior studies demonstrate the sensitivity of hydrologic and coupled ecohydrologic processes to temperature patterns, suggesting that a bias in temperature interpolation may significantly impact assessments of climate impacts. Analysis of model prediction sensitivity to different temperature interpolation approaches is needed to provide guidelines for the use and interpretation of ecohydrologic models in climate change assessment.

[5] For hydrologic models, significant temperature interpolation bias should be apparent in comparisons of model predicted streamflow against observed streamflow data. Hydrologic models, however, are also calibrated against observed streamflow data; therefore, calibration may obscure the effects of temperature interpolation bias. Because distributed hydrologic models are often limited by data that describe soil hydraulic and subsurface drainage properties, these properties become calibration parameters [*VanRheenen et al*., 2004; *Christensen et al*., 2004; *Hamlet et al*., 2005; *Jung and Chang*, 2011]. In general, calibration may bias drainage parameter estimates to compensate for the errors in input data [*Kirchner*, 2006; *McDonnell et al*., 2007]. Thus, the error associated with air temperature estimates may influence model calibration and lead to inaccurate estimates of subsurface drainage parameters. For example, if errors in temperature lapse rates lead to earlier snowmelt predictions, calibration against observed streamflow may select for slower drainage parameters to compensate for the effect of the early snowmelt timing. Drainage parameters can be assumed to remain stationary under a changing climate. We expect, however, that given the importance of temperature as a control on snow accumulation and melt, temperature lapse rate errors may change under climate-warming scenarios if minimum and maximum temperatures change at different rates or, in regions with cold-air pooling events, with changes in frequency of anticyclonic conditions [*Daly et al*., 2010]. Thus, any bias introduced into drainage parameters during calibration as a result of inaccurate temperature lapse rates will be problematic when the model is used to develop climate-warming scenarios. Further evaluation of models using streamflow data provides information only on total basin water balance. Streamflow assessment may not reflect the influence of temperature lapse rate bias on predictions of within watershed patterns of ecohydrologic processes, including forest transpiration and NPP, that are expected to be sensitive to climate variability and change.

[6] In this paper we compare five methods of surface temperature approximation and the associated sensitivity of model estimates for streamflow, snow dynamics, transpiration, and productivity in a mountain environment. We use the Regional Hydro-Ecological Simulation System (RHESSys) [*Tague and Band*, 2004], a process-based model, to simulate coupled ecohydrologic processes. We focus our study in the HJ Andrews Experimental Forest (HJA), which has been shown to have cold-air pooling and drainage and strong, seasonally varying temperature inversions [*Daly et al*., 2007, 2010]. Thus, the HJA, which is dominated by a rain-snow transition zone, is likely to be particularly sensitive to spatial-temporal patterns of air temperature. We compare model estimates calculated using a standard, temporally constant mean temperature lapse rate of $-6.5°C\ km^{-1}$, two daily temperature lapse rates derived from local climate stations within the basin, and temperatures estimated using two resolutions of PRISM temperature data [*Daly et al*., 2002; *Smith*, 2002]. These five scenarios allow for comparison of (1) linear temperature interpolation methods to PRISM's nonlinear, spatially distributed interpolation; (2) sensitivity in temperature estimates to the location of the meteorologic station used to derive temperature lapse rates; and (3) sensitivity to resolution of PRISM's spatially distributed data. We use each of these methods to provide temperature input data to RHESSys and compare both model calibration behavior and postcalibration estimation of streamflow, forest water use, and productivity under historic climate variability.

2. Methods

2.1. Study Area

[7] The HJA is a Long Term Ecological Research site located in the western Cascade Range of Oregon, USA.

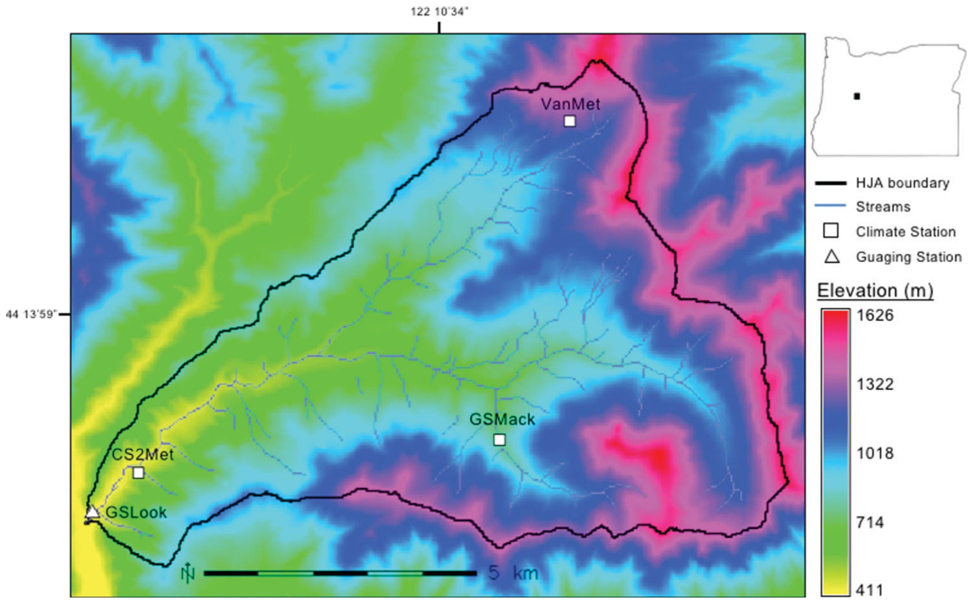

Figure 1. The 30 m digital elevation map of the HJA located in Oregon, USA. Geographic locations of climate stations used to calculate daily temperature lapse rates for 2PT-LOW (CS2MET, VANMET) and 2PT-MID (GSMACK, VANMET) are shown as white squares.

Elevations in the 64 km^2 basin range from 410 to 1630 m (Figure 1). The forested basin is dominated by conifers with *Tsuga heterophylla* (western hemlock) at lower elevations, *Abies amabilis* (Pacific silver fir) at higher elevations, and *Pseudotsuga menziessi* (Douglas-fir) throughout the whole basin [*Franklin and Dyrness*, 1988]. It has a Mediterranean climate with wet winters and dry summers where approximately 75% of the annual precipitation falls from November to April. Located on the windward slope of the Cascade Range, the HJA receives orographically enhanced precipitation that typically increases with elevation, and a substantial seasonal snowpack develops above 900 m. The HJA's steep, incised slopes and valleys create periods of cold-air drainage and pooling. Negative radiation balance and slow wind speeds result in temperature inversions near the ground that switch to a typical temperature profile above the inversion [*Daly et al*., 2007]. Estimates of ecohydrologic values are likely to be particularly sensitive to temperature interpolation scenarios in the HJA given that it is located in a rain-snow transition zone and is prone to cold-air pooling and temperature inversions.

2.2. Model Description

[8] RHESSys is a spatially distributed, dynamic model of water, carbon and nitrogen fluxes over spatially variable terrain. *Tague and Band* [2004] describe the model's original process representations; however, the model is continually evolving, and version 5.14.4 is used in the work presented here. RHESSys uses a hierarchical spatial framework that allows different processes to be modeled at their most representative scale [*Band et al*., 2001]. For this study the resolution for meteorologic, hydrologic, and carbon cycling processes is similar across temperature lapse rate scenarios. We use patch sizes of 30 m^2 for the three non-gridded temperature scenarios and 50 m^2 for PRISM-derived temperatures. Daily minimum and maximum air temperatures and precipitation inputs drive the biogeochemical cycling and hydrologic flux estimates. Here we give a brief overview to highlight how air temperature inputs influence model estimates of ecohydrologic variables. Daily partitioning of incoming precipitation between rain and snow is based on each grid's air temperature and assumes that all precipitation falls as snow below $-2°$C and as rain above 2°C based on previously reported observations [*U.S. Army Corps of Engineers*, 1956; *Daly et al*., 2007], with a linear partitioning for temperature between $-2°$C and 2°C based on the average daily temperature. Snowmelt is modeled using a combined energy budget and temperature index similar to the approach used by *Coughlan and Running* [1997]. Temperature is also used to calculate potential evapotranspiration. Approaches used to estimate daily litter, soil, and canopy interception and evaporation as well as transpiration are based on Penman or Penman-Monteith approaches. If vapor pressure deficit (VPD) data are not available (as is commonly the case in the application of hydrologic models), then VPD is estimated using the average air temperature, calculated using the daily minimum and maximum air temperature, following *Jones* [1992]. Because VPD is sensitive to air temperature, modeled evapotranspiration estimates will also show some sensitivity to air temperature. Stomatal conductance is estimated using a Jarvis approach, which includes an air temperature response function. Transpiration also varies with soil water availability, which changes with recharge from snowmelt. Gross photosynthesis is estimated using the Farquhar approach and includes a temperature term; and following the approach used by *Ryan* [1991], respiration of different plant components increases with temperature. Infiltration and soil moisture storage and drainage all respond to the timing and magnitude of recharge, which includes snowmelt. Streamflow is generated through a combination of lateral hillslope routing of saturation

excess, shallow subsurface flow, and deeper groundwater flow as described by *Tague et al*. [2008].

[9] For this study we assume a mature Douglas-fir stand for estimates of gross and net photosynthesis, respiration, and transpiration. To initialize carbon and nitrogen pools for the forest, vegetation, soil, and litter, we ran RHESSys for the HJA over a 300 year climate sequence, created by repeating a 50 year (1957–2007) record. For comparisons of ecohydrologic estimates across the five different temperature estimation scenarios (described in detail later), we used the same initial state (carbon, nutrient stores) and ran the model for water years 1991–2000, where a water year is defined as 1 October of the previous year through 30 September of the present year. For these comparisons, the model was calibrated in static mode, where carbon and nutrient stores do not change throughout the simulation. This allowed us to compare vegetation responses (NPP and transpiration) in individual years given the same stand structure.

[10] The model was calibrated against a daily streamflow record obtained from stream gauge station GSLOOK (U.S. Geological Survey (USGS) gage 14161500). A primary source of uncertainty in hydrologic modeling is the characterization of basin-wide soil properties [*Freer et al*., 2002; *Beven and Freer*, 2001]. While other hydrologic model parameters can be directly measured, subsurface drainage and moisture storage properties are influenced by both soil matrix properties and distributions of preferential flow paths and macropores over depth, which cannot be directly measured. Consequently, subsurface drainage parameters are almost always calibrated for or inferred by parameter transfer from other regions of similar geology [*Beven*, 1989, 1996]. Similar to previous applications of RHESSys [*Tague et al*., 2004; *Tague and Grant*, 2009], calibration was achieved by adjusting parameters that control storage and drainage rates of water through the soil and subsurface. We calibrate for six parameters. The upper and lower limits of each parameter's values are bounded by literature estimates [*Dingman*, 1994]. We emphasize that the realistic ranges for K and m are large due to the presence of macropores and preferential flow paths [*Rothacher et al*., 1967; *Harr*, 1977; *McGuire and McDonnell*, 2010]. RHESSys distinguishes between shallow subsurface flow paths that follow surface topography and interact with the vegetation rooting zone, and deeper groundwater flow paths that bypass the rooting zone and are organized at broader hillslope scales. In the shallow subsurface flow system, soil air-entry pressure (ae) and pore size index (po) control the soil water holding capacity, following the approach of *Brooks and Corey* [1964]. Saturated hydraulic conductivity at the surface (K) and its decay with depth (m) control vertical and lateral shallow subsurface drainage rates. Storage and routing to a deep groundwater store requires two groundwater (gw) parameters: the first (gw1) represents a fixed percentage of infiltrated water that is assumed to bypass the soil matrix to the deep groundwater store, and the second (gw2) represents the amount that is routed to the stream at a calibrated drainage rate.

[11] Calibration was done separately for each of the five temperature interpolation approaches. We used a Monte-Carlo-based approach with 1000 simulations over a 10 year period, water years 1991–2000, with an initial spin-up in water year 1990. Acceptable parameter sets were selected based on the three metrics of model performance against measured streamflow. Specifically, the Nash-Sutcliffe efficiency (NSE) of daily streamflow and log-transformed daily streamflow were held to greater than 0.6 [*Nash and Sutcliffe*, 1970], annual absolute values of streamflow bias were less than 15%, and August streamflow biases, considered a low-flow month, were less than 25%. A single parameter set was selected from these acceptable parameter sets for each temperature scenario to illustrate differences in modeled streamflow, snow accumulation, and melt.

[12] For model evaluation, we expand the three performance measures mentioned earlier. Although calibration could include additional statistics, calibration of most hydrologic models and previous RHESSys applications [*Seibert et al*., 1997; *Hay and Clark*, 2003; *Tague et al*., 2004] typically focuses on a smaller subset. We use other performance measures in evaluation, however, to provide a more detailed analysis of hydrologic behavior. We focus particularly on spring and summer flows and compute the root-mean-square error (RMSE) and bias in these seasonal totals. Spring and summer flows are likely to be most sensitive to temperature controls on snowmelt and evapotranspiration, respectively. Following *Stewart et al*. [2004], we also compute the day of water year of the center of mass of streamflow (DofCM), which reflects the timing of spring snowmelt in environments where water inputs are dominated by winter snow. The DofCM is the day of water year in which 50% of the total annual streamflow has been discharged from the basin.

2.3. Model Inputs

[13] Elevation, slope, and aspect layers for the HJA were based on a 30 m digital elevation model (available at http://www.fsl.orst.edu/lter). Daily minimum and maximum temperature records were taken from three stations within the basin: Climatic Station at Watershed 2 (CS2MET), located in a valley bottom at 430 m elevation; Andrews Mack Creek Gaging Station (GSMACK), located at 755 m elevation; and the high-elevation Vanilla Leaf Meteorological Station (VANMET), located at 1273 m elevation (Figure 1). Precipitation records from CS2MET were scaled using isohyets derived from 800 m PRISM data and used to drive all model scenarios.

[14] 2.3.1. Temperature Estimation Scenarios We compare two general approaches, linear interpolation and PRISM-derived temperature maps, for providing spatially explicit temperature inputs to RHESSys. It has been shown that accuracy in temperature estimation is heavily influenced by sensor location [*Stahl et al*., 2006]. In addition, it has been shown that the HJA is prone to decoupling between cold-air pools and free atmosphere at higher elevations [*Daly et al*., 2010], leading to fall and winter temperature inversions. Using a MALR is likely to underestimate high-elevation temperature data during periods of temperature inversion or cold-air pooling. Temperature lapse rates derived from station pairs, on the other hand, can account for these time-varying controls on temperature patterns, but results will depend on local effects at the respective pairs. We examine three linear interpolation scenarios to derive daily minimum and maximum temperature lapse rates. The first approach applies a temporally constant MALR of

Table 1. Naming Convention of Temperature Interpolation Methods

Abbreviation	Data Used to Derive Minimum/Maximum Temperature Lapse Rates
MALR	Mean adiabatic lapse rate; constant value of 6.5°C km^{-1}
2PT-LOW	Linear interpolation with CS2MET (low) and VANMET (high)
2PT-MID	Linear interpolation with GSMACK (mid) and VANMET (high)
GRID-50	50 m resolution PRISM-derived grids
GRID-800	800 m resolution PRISM-derived grids

-6.5°C km^{-1} to daily minimum and maximum temperatures and acts as a baseline. This lapse rate is applied to temperature values recorded at CS2MET for model data input. This scenario is referred to as MALR throughout the article. Table 1 lists all scenarios' acronyms and descriptions.

[15] The two other temperature estimation scenarios that use linear interpolation allow spatial patterns of temperature to vary through time. Daily time series of minimum and maximum temperature lapse rates were calculated for water years 1990–2000 using distinct daily minimum and maximum temperatures from high- and low-elevation stations. Both scenarios use VANMET as the high-elevation station. Low-elevation station CS2MET, located on the valley floor, and mid-elevation station GSMACK are used to calculate the daily temperature lapse rates for scenarios 2PT-LOW and 2PT-MID, respectively. We apply the 2PT-LOW and 2PT-MID lapse rates to the temperature data recorded at their respective individual low-elevation meteorologic stations, CS2MET and GSMACK. These basin-wide daily temperature lapse rates were calculated as

$$\Gamma_{\text{2PT-LOW}\,\max,\min} = \frac{T_{\text{VANMETmax,min}} - T_{\text{CS2METmax,min}}}{Z_{\text{VANMET}} - Z_{\text{CS2MET}}} \quad (1)$$

$$\Gamma_{\text{2PT-MID}\,\max,\min} = \frac{T_{\text{VANMETmax,min}} - T_{\text{GSMACKmax,min}}}{Z_{\text{VANMET}} - Z_{\text{GSMACK}}}, \quad (2)$$

where T is the daily temperature, Z is the elevation, and $\Gamma_{\max,\min}$ are the change in maximum and minimum temperatures with elevation, respectively (i.e., daily lapse rate). Figure 2 shows the daily average temperature lapse rates averaged across 11 water years (1990–2000). In the HJA, $\Gamma_{\max}$ for scenarios 2PT-LOW and 2PT-MID approximates the global mean temperature lapse rate of -6.5°C km^{-1} during spring and summer. During the fall and winter, both scenarios' lapse rates demonstrate strong temperature inversions. During the periods of inversion $\Gamma_{\text{2PT-MIDmax}}$ is on average 3°C higher than $\Gamma_{\text{2PT-LOWmax}}$. The steeper temperature lapse rate computed using the mid- and high-elevation station pair is somewhat surprising given that we might expect the temperature inversions effect to be greater from the lower-elevation station. Results indicate that the 2PT-MID elevation pair actually shows a strong temperature inversion effect. There is a negligible difference between $\Gamma_{\min}$ for 2PT-LOW and 2PT-MID; both average -3.5°C km^{-1}, or 3°C km^{-1} higher than the mean environmental lapse rate. Detailed analysis of the HJA climate is

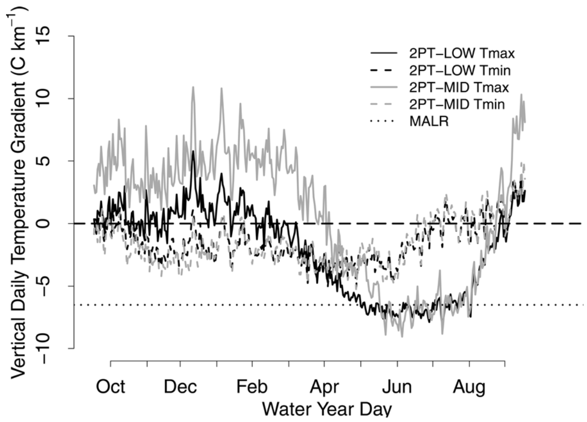

Figure 2. Time series of $\Gamma_{\text{2PT-LOWmin,max}}$ and $\Gamma_{\text{2PT-MID-min,max}}$ averaged over water years 1990–2000, expressed in C km^{-1} vertical elevation. Gray lines represent Γ for 2PT-MID; black lines represent 2PT-LOW; and dashed and solid lines are minimum and maximum lapse rates, respectively. A horizontal line at $\Gamma = 0$ is included to aid in identification of inversion periods.

beyond the scope of this paper; here we focus on the implications for ecohydrologic estimates. *Daly et al*. [2010] provide a more detailed analysis of the climate mechanisms that controls these rates and their climatic and seasonal patterns.

[16] We also consider two temperature interpolation scenarios that use spatially explicit, long-term (1971–2000) monthly averages of minimum and maximum temperature created with PRISM. We compare scenarios based on PRISM at a resolution of 800 m, which is available for all of the contiguous United States, and scenarios based on 50 m resolution maps that are unique to the HJ Andrews (available at www.fsl.orst.edu/lter/data/abstract.cfm?dbcode=MS029) [*Smith*, 2002; *Daly and Smith*, 2005]. PRISM-based temperature estimates account for environmental factors such as forest canopy, cloudiness, and topographic shading of radiation that are known to affect microclimates in forested, high topography terrain. These gridded temperature data are able to capture temperature inversions and thermal belts because PRISM weighs climate stations to account for topographic positioning and potential for temperature inversion [*Daly et al*., 2008]. We use the same methodology, detailed later, to incorporate 50 and 800 m resolution data into RHESSys and refer to these scenarios as GRID-50 and GRID-800, respectively.

[17] To generate daily estimates for both data sets, the monthly data were downscaled into grids of daily maximum and minimum temperature for years 1989–2000 using the CS2MET record. First, the raw, monthly temperature values were offset with respect to the corresponding monthly value for the grid cell at the CS2MET climate station.

$$\text{oMPT}_{j(\max,\min),i} = \text{MPT}_{j(\max,\min),i} - T_{\text{CS2MET}\,(\max,\min),i}. \quad (3)$$

[18] We denote monthly, PRISM-derived minimum or maximum temperatures for grid cell j at month i as $\text{MPT}_{j,i}$. The mean monthly PRISM temperature value of the grid cell that is coincident with the geographic location of

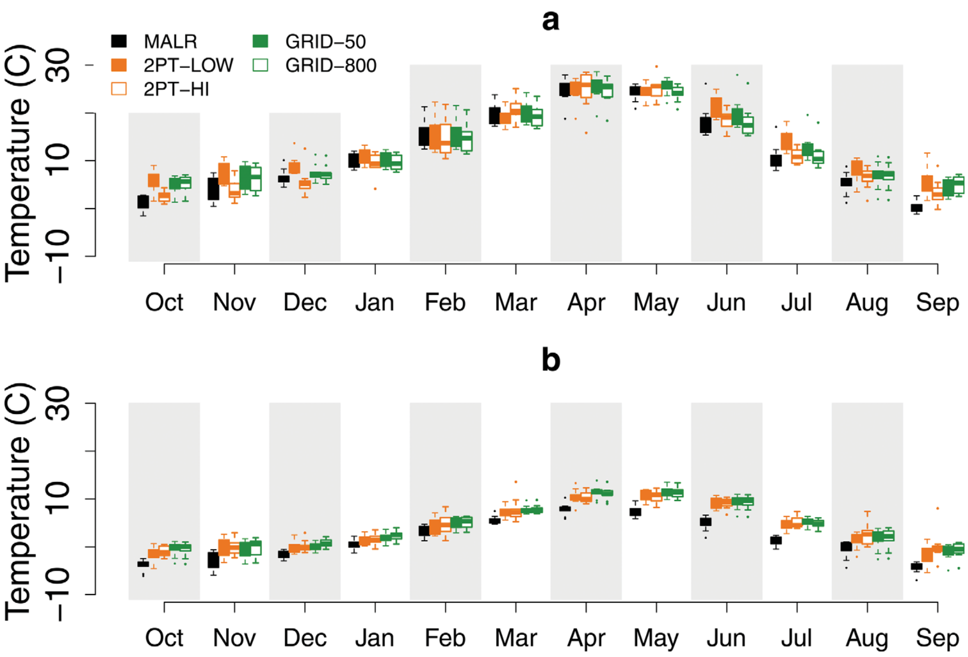

Figure 3. Monthly (a) maximum and (b) minimum temperatures averaged over the basin and water years 1991–2000. For each month, bars from left to right represent scenarios MALR, 2PT-LOW, 2PT-GRID, GRID-50, and GRID-800.

climatic station CS2MET is $T_{\mathrm{CS2MET},i}$, and $\mathrm{oMPT}_{j,i}$ represents the gridded temperature values offset by $T_{\mathrm{CS2MET},i}$ for month i at grid cell j. The daily minimum and maximum temperature records from CS2MET ($\mathrm{CS2MET}_{\mathrm{max,min}}$) are used to downscale the monthly $\mathrm{oMPT}_{j,i}$ to a daily time step.

$$\mathrm{DoMPT}_{j(\max,\min),i,k} = \mathrm{oMPT}_{j(\max,\min),i} + \mathrm{CS2MET}_{\max,\min i,k}. \quad (4)$$

[19] We use $\mathrm{DoMPT}_{j(\max,\min),i,k}$ to refer to the product of adding grid oMPT at month i to CS2MET's temperature value in the same month on day k.

3. Results

3.1. Average Monthly Basin Temperatures

[20] Figure 3 shows the monthly temperature values averaged over the basin and climate record for each of the five methods of estimation. The MALR estimated the lowest maximum and minimum temperatures throughout the growing season. Mean basin summer and fall maximum temperatures for 2PT-LOW were on average the highest estimates of all scenarios (Figure 3a). GRID-800 maximum temperatures were generally cooler than estimates from finer resolution GRID-50. Minimum temperature estimates (Figure 3b) for all scenarios showed the greatest differences across temperature estimation methods in April–October and the greatest interannual variation in November. When averaged over the basin, differences in monthly estimates due to interpolation approaches were small when compared with seasonal patterns in air temperature (e.g., differences between winter and summer temperatures) but were relatively large when compared with interannual variation of air temperature for a particular month (e.g., shown by height of bars in Figures 3a and 3b).

3.2. Model Calibration and Performance

[21] The method of temperature estimation influenced both the number of acceptable parameter sets and the performance statistics values of the best performing parameters. Of all scenarios, 2PT-MID had the greatest number of acceptable parameter sets (Table 2). Of the spatially distributed interpolation methods, GRID-50 had the most parameter sets meeting streamflow metric criteria (Table 2). GRID-50 and 2PT-MID had more than twice as many acceptable parameter sets as compared to the other three scenarios. We suggest that the need to correct for temperature effectively imposed an additional constraint and reduced the number of acceptable parameters. The effect of temperature estimation on model calibration was also reflected in the differences of acceptable parameter values. Four of the six calibration parameters demonstrate distinct parameter spaces for each temperature scenario (Figure 4). All linear interpolation scenarios (MALR, 2PT-LOW, and 2PT-MID) selected for a greater proportion of flow to deeper groundwater stores (minimum value of 0.1 in Figure 4c), shown as deviation in cumulative distribution of

Table 2. Total Number of Parameter Sets That Satisfy the Following Daily Streamflow Performance Metrics From the Original 1000 Calibration Parameters[a]

Scenario	Total
MALR	20
2PT-LOW	10
2PT-MID	67
GRID-50	54
GRID-800	26

[a]NSE > 0.6, NSE log > 0.65, total error <15%, error in August <25%.

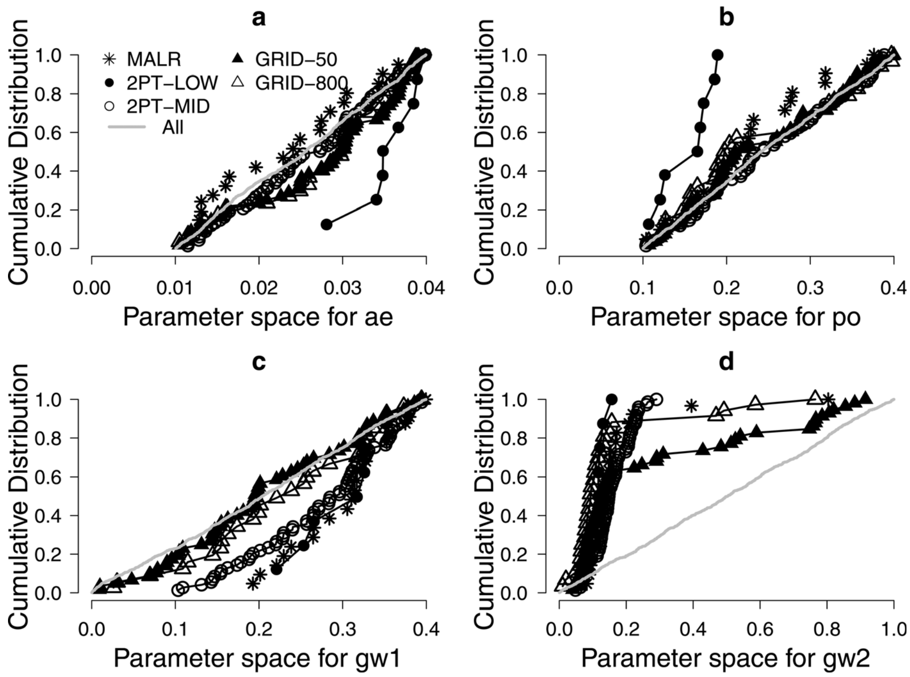

Figure 4. Cumulative frequency analysis of calibration parameters (a) ae, (b) po, (c) gw1, and (d) gw2 for the five temperature estimation scenarios. For each scenario, the parameter value meeting streamflow metrics listed in Table 2 is plotted against the normalized value of log(NSE). The parameter space for all 1000 initial parameter sets is shown with the gray line.

acceptable parameters from cumulative distribution of the initial parameter space, following *Beven and Freer* [2001]. Higher values of gw1 reflect an implementation where a greater proportion of recharge follows a shallow (and relatively rapid) groundwater flow path. These linear interpolation scenarios also selected for slightly lower values of gw2, leading to faster drainage rates of the deeper groundwater store (maximum value of 0.4 in Figure 4d). GRID-800 selected for gw1 parameters intermediates between GRID-50 and the linear interpolation scenarios. With respect to the timing of streamflow, slower drainage of the deeper groundwater stores in MALR, 2PT-LOW, and 2PT-MID partially (but not fully) compensates for a greater proportion of recharge traveling through the deeper (rather than shallow subsurface) flow paths (higher gw1). Partitioning of recharge into the deeper versus shallow groundwater flow can also influence evapotranspiration rates because water that remains in the shallow subsurface flow system can be accessed for transpiration by downslope vegetation, particularly in riparian areas. Thus, linear interpolation scenarios may be selecting for greater partitioning into groundwater stores to reduce growing-season evapotranspiration rates.

[22] Scenario 2PT-LOW also selected for a narrow range of values for po and ae (Figures 4a and 4b); the smaller pore size indices and higher air-entry pressure, values that reflect reduced soil moisture storage capacity, likely lead to lower growing-season evapotranspiration rates. In general, 2PT-LOW parameters suggested compensation to correct for a tendency toward higher evapotranspiration rates by reducing soil moisture storage capacity. Though we calibrated for parameters *m* and *K*, the difference in acceptable parameter space between temperature estimate scenarios differed little, so they are not shown.

[23] A single acceptable parameter set was selected for each scenario in order to illustrate differences in postcalibration ecohydrologic variable estimates across the temperature scenarios. These parameter sets are presented in Table 3. Where possible, parameter sets were chosen to be similar across temperature scenarios, while still meeting the calibration criteria for acceptability. There was no unique parameter set common to all five scenarios. MALR, 2PT-MID, GRID-50, and GRID-800 scenarios share a common parameter set meeting streamflow metrics; 2PT-LOW has a separate, distinctive parameter set, chosen such that its values of gw1, ae, and po were within 25% of the other common parameter set so as to minimize differences in soil moisture storage and total volume of water lost to deep groundwater.

3.3. Streamflow

[24] Once calibrated, streamflow estimates from all five temperature scenarios achieved performance statistics for annual and daily flows (Table 4) that were similar to those

Table 3. Calibrated Soil Parameters Used for the Presentation of Modeled Streamflow and Snowpack for Each Temperature Estimation Method in All Scenarios

Scenario	m (m^{-1})	K (m d^{-1})	po	ae	gw1	gw2
MALR, 2PT-MID, GRID-50, GRID-800	1.18	2180	0.28	.015	0.33	0.13
2PT-LOW	1.24	3250	0.18	0.019	0.25	0.08

Table 4. Daily Streamflow Performance Metrics for Each Temperature Scenario Computed for Water Years 1991–2000

	Daily Streamflow Performance Metrics		
Scenario	Bias (%)	NSE	log(NSE)
MALR	−5.1	0.61	0.81
2PT-LOW	−10.1	0.62	0.83
2PT-MID	−6.3	0.69	0.85
GRID-50	−7.3	0.65	0.87
GRID-800	−11.7	0.60	0.85

used for previous hydrologic modeling studies in the western United States [*Hay and Clark*, 2003; *Hay et al.*, 2006; *Tague and Grant*, 2009]. There were, however, some noticeable differences in performance statistics across temperature scenarios. Table 4 shows daily streamflow metrics for water years 1991–2000 and demonstrates that in all scenarios timing of magnitude was reasonably captured. Table 5 shows metrics for seasonal streamflow, highlighting periods of high (spring) and low (typically August) flows.

[25] Overall, 2PT-MID and GRID-50 modeled the timing and amount of streamflow slightly better than the other linear or spatially distributed interpolations across all time scales, based on a range of streamflow metrics (Tables 4 and 5). Although 2PT-LOW had relatively low bias in seasonal (fall and spring) totals, there was a substantial bias toward earlier streamflow (earlier DofCM), leading to a high RMSE in the spring (Table 5). Timing of center of mass of streamflow for MARL, 2PT-MID, GRID-50, and GRID-800 was substantially biased toward later in the season. The 2PT-MID had a lower RMSE for the spring. GRID-50 and GRID-800 similarly had a higher spring RMSE and the lowest fall RMSE. MALR gave the poorest performance with spring and fall biases of approximately 20%, nearly 2–20 times greater than the other scenarios. Monthly streamflow patterns (Figure 5) show that MALR predicted a slightly more muted seasonality with reduced differences between wet and dry season flows. For MALR, the mean flows in wet months were approximately 10 mm d^{-1}, and flows in the dry summer months were 2 mm d^{-1}. Figure 6 presents a hydrograph for water year 2000, a year of average annual precipitation, to illustrate the difference in scenarios' abilities to capture peak flows and recessions. It shows that MALR underestimated early winter discharge and overestimated summer low flows. Linear interpolation

Table 5. Seasonal (Fall and Spring) Streamflow Performance Metrics for Each Temperature Scenario Computed for Water Years 1991–2000

	Spring, Mar–Apr–May			Fall, Low Flow	
Scenario	RMSE (mm)	Bias (%)	Average Number of Days Removed From Observed DofCM	RMSE (mm)	Bias (%)
MALR	16.8	18.3	20 later	11.9	−21.6
2PT-LOW	16.7	−1.0	10 earlier	8.4	−1.3
2PT-MID	8.8	−3.7	12 later	8.0	6.5
GRID-50	12.1	−2.1	9 later	7.3	−14.3
GRID-800	11.6	−5.8	11 later	7.3	−13.9

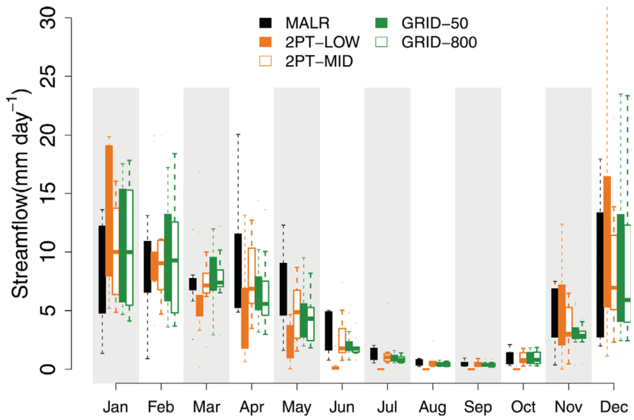

Figure 5. Average monthly streamflow for water years 1991–2000 for all temperature interpolation scenarios. For each month, bars from left to right represent scenarios MALR, 2PT-LOW, 2PT-GRID, GRID-50, and GRID-800.

scenario 2PT-LOW (Figure 6b) underestimated flow from March to July and overestimated peak flows. In water year 2000, both GRID-50 and GRID-800 (Figure 6c) have similar performance and tend to slightly underestimate peak flow values. In spite of these differences among scenarios, we emphasize that all produce similar daily streamflow statistics (NSE, log(NSE)) and acceptable streamflow performance. (A log(NSE) value of greater than 0.8 suggests that a scenario captures general hydrologic behavior (peaks, low flows, seasonality) reasonably well.) Figure 7a shows that MALR's DofCM occurred later than observed for all years and 2PT-LOW occurred earlier than the observed record for all years except for 1993, which was the year of latest spring peak discharge. All scenarios follow the general trends in interannual variation in timing of center of mass, with 1993 showing the latest timing of melt and 1997 the earliest.

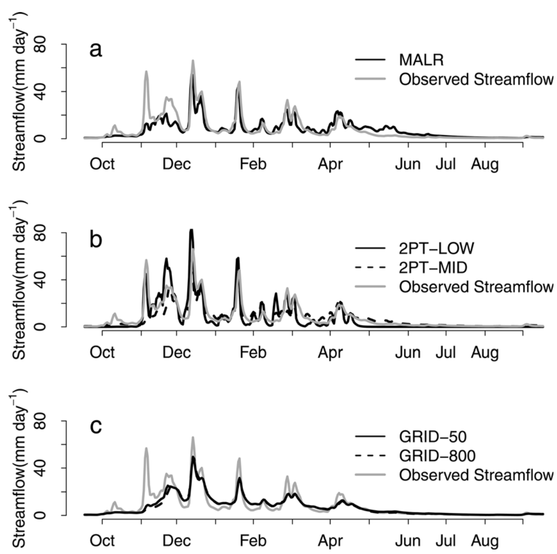

Figure 6. Modeled streamflow for water year 2000, a year of average annual precipitation (over record 1957–2005), illustrates differences in seasonal timing using the five temperature scenarios.

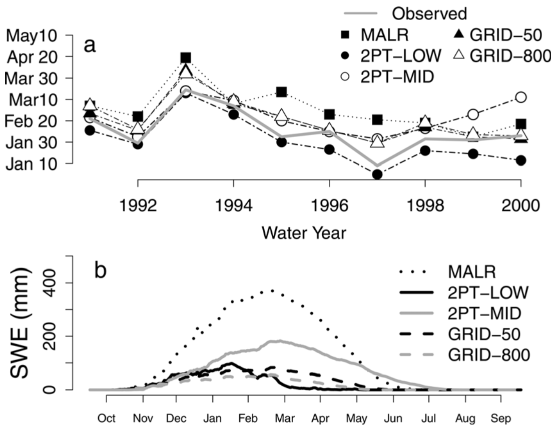

Figure 7. Differences in temperature interpolation affect modeling of snow processes such as (a) timing of snowmelt, reflected here as streamflow's DofCM where points modeled above the gray line (observed) indicate delay in melt, and (b) magnitude, shown as the 10 year average SWE.

3.4. Snow

[26] Model prediction of the timing and amount of snow is particularly sensitive to temperature strategies. As mentioned earlier, Figure 7a shows the influence on timing using the DofCM; Figure 7b shows the daily snow water equivalent (SWE) for water years 1991–2000 to illustrate differences in accumulation. The MALR strategy calculated a peak mean basin SWE of 400 mm, two to four times the amount calculated by any other basin-specific strategy. Four SNOTEL stations near the HJA at elevations from 1140 to 1460 m recorded peak snowpacks ranging from 100 to 900 mm (data not shown). We note that basinwide estimates of SWE are not generally available, and remote sensing of SWE is challenging in densely forested watersheds [*Bales et al*., 2006]. Thus, we consider model estimates of basin-wide average SWE to all be reasonable within a first-order approximation despite distinct differences in estimates with temperature strategies. The magnitudes of peak SWE estimated by 2PT-LOW, GRID-50, and GRID-800 were roughly equivalent; however, GRID-50 and GRID-800 have a later average day of peak SWE and slower melt rates; GRID-50 shows slightly higher peak snow. The 2PT-MID peak snow was substantially greater than that estimated by 2PT-LOW or GRID-50. Basin-average snowpack accumulation peaks occurred at notably different times: 2PT-LOW occurred in January, 2PT-MID and MALR peak in February, and the gridded scenarios' snowpacks shared a much smoother peak in late February. Differences in peak SWE estimates have implications for timing of snowmelt. MALR's larger snowpack strongly influences its 20 day delay in DofCM (Table 5 and Figure 7a), and similarly, 2PT-MID's and the gridded scenarios' approximate 10 day delay in DofCM reflects their later melt.

3.5. Ecologic Modeling: Transpiration and Carbon Cycling

[27] Transpiration and NPP estimates presented are for all parameter sets that met streamflow metrics of acceptability (Table 2). Mean annual transpiration and NPP for all temperature lapse rate scenarios were between 580 and 800 mm yr^{-1} and 450 and 2000 g C yr^{-1} (Table 6), respectively; GRID-800 and 2PT-MID estimated very high mean annual NPPs of approximately 2000 g C m^{-2}, and MALR had an NPP estimate of 450 g C m^{-2}, approximately one quarter the magnitude of GRID-800. MALR modeled the lowest rates of growing-season transpiration (approximately 4 mm d^{-1}) and the greatest interannual variation in its estimates of transpiration and NPP (Table 6), which implies a greater sensitivity to year-to-year differences in climate forcing. In contrast, GRID-50 and 2PT-LOW had the smallest interannual variability in NPP and transpiration estimates, respectively. NPP estimates using the five different temperature lapse rate scenarios also differed in their sensitivity to uncertainty in soil drainage parameters (Figures 8a and 8b). The variability in NPP and transpiration across acceptable parameter sets by 2PT-MID was relatively small given that it reflects estimates of 67 parameters as compared to 21 (MALR) or 10 (2PT-LOW; Figures 8a and 8b). Figures 8a and 8c also show that the differences in total annual NPP and transpiration across scenarios largely reflect differences in late summer fluxes. MALR, having the lowest annual estimates of NPP, shows the earliest and steepest declines in summer transpiration and NPP, reflecting an earlier onset of summer water stress (Figures 8a and 8c). Similarly, as shown in Figure 8c, the timing in seasonal peaks of transpiration for 2PT-MID, GRID-50, and GRID-800 distinguishes these scenarios' higher rates of total annual (approximately 760 mm yr^{-1}) transpiration from MALR and to a lesser extent, 2PT-LOW. Maximum daily rates of estimated transpiration by GRID-800 peaked at approximately 7 mm d^{-1} in July, 2 mm higher and 2 months later than MALR.

Table 6. Mean Annual Values of NPP and Transpiration for the Parameter Sets Meeting Streamflow Metrics Listed in Table 2

Temperature Scenario	Mean Annual NPP (g C m^{-2})	Standard Deviation of Annual NPP (g C m^{-2})	Mean Annual Transpiration (mm yr^{-1})	Standard Deviation of Annual Transpiration (mm yr^{-1})
MALR	450	230	580	80
2PT-LOW	930	80	730	30
2PT-MID	1900	120	760	80
GRID-50	1540	70	760	50
GRID-800	2000	80	800	50

4. Discussion

[28] Accurate modeling of ecohydrologic processes in mountainous terrain relies strongly on capturing seasonal snow patterns. Temperature interpolation methods have the potential to play a strong role in improving representation of snow accumulation and melt in regions with warm winters. Watersheds with large rain-snow transition zones such as the HJA study site are likely to be particularly sensitive to temperature estimates. We assume here that the GRID-50 scenario is the most physically realistic of the temperature scenarios because it is derived using PRISM at a fine resolution by using more than 30 temperature sensors within the basin [*Smith*, 2002]. Thus, it is

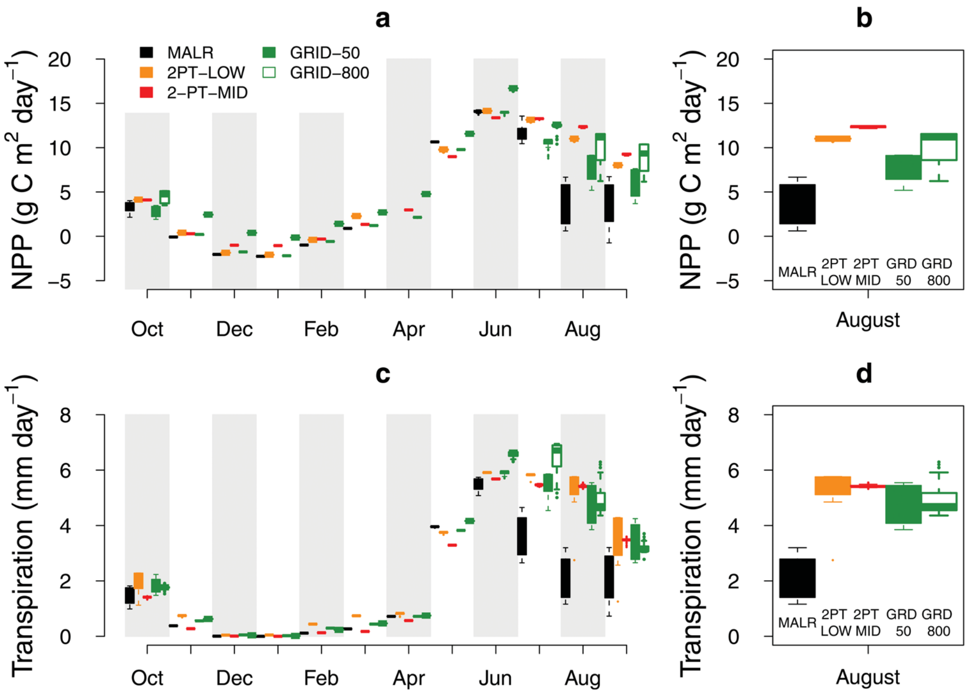

Figure 8. Ten year monthly averages of modeled (a) NPP and (b) transpiration for the parameter sets that meet streamflow metrics listed in Table 2. August averages for (b) NPP and (d) transpiration allow for closer inspection of differences in model estimates. For each month, bars from left to right represent scenarios MALR, 2PT-LOW, 2PT-GRID, GRID-50, and GRID-800.

most likely to capture spatial variation in air temperature lapse rates and reflect the seasonal, atmospheric decoupling that occurs in the basin. We note that a limitation of GRID-50 is that because daily gridded values were unavailable, it is downscaled from a monthly-to-daily time step using data from low-elevation station CS2MET. So though GRID-50 provides improved spatial information about the HJA temperature regime, 2PT-LOW and 2PT-MID have the advantage of providing daily lapse rates, which may facilitate capturing daily processes like cold-air pooling. We note however that winter temperature inversions are still captured at the monthly time scale. The best postcalibration streamflow performances (percent daily bias, DofCM, and low-flow bias) were obtained using the 2PT-MID and GRID-50 scenarios, and these scenarios had the greatest number of acceptable parameter sets. These behaviors lend confidence to our ranking of GRID-50 as the most realistic temperature scenario.

[29] The standard atmospheric environmental lapse rate (MALR) modeled two to four times greater snow accumulation than all other scenarios. We suggest that this is explained in part by MALR's winter lapse rates not capturing the inversion that exists in the HJA and that $-6.5°\text{C km}^{-1}$ is not representative of mountainous terrain in the Pacific Northwest [*Minder et al.*, 2010]. MALR's steeper winter temperature lapse rates effectively lower the average basin temperatures and thus partition a larger fraction of winter precipitation to snow. Differences in the fraction of winter precipitation as snow can translate into significant differences in runoff [*Minder et al.*, 2010; *White et al.*, 2002]. In these results, MALR shows a 3 week delay on average in peak spring flow and higher average amounts of late summer streamflow. Scenario 2PT-MID also had a higher peak SWE that occurred later in the year than the other basin-specific linear interpolation, 2PT-LOW, and grid-based approaches. Differences between 2PT-LOW and 2PT-MID highlight the impact of temperature sensor location on ecohydrologic model estimates, even when time-varying lapse rates with elevation are accounted for and stations are selected to capture high-to-low elevation behaviors. The slightly greater amount of snow accumulation by GRID-50 than by GRID-800 suggests that the finer resolution temperature maps better capture cold-air pockets in the HJA.

[30] In spite of substantial difference in snow estimates, calibration of drainage parameters to some extent compensates for the impact of snowmelt timing on streamflow. We note, however, that while acceptable NSE and log(NSE) were obtained for all scenarios, closer examination of seasonal patterns of streamflow does reflect the differences in snow estimates, even after calibration. The later snowmelt timing of the MALR, 2PT-MID, and the gridded interpolation scenarios remains evident in streamflow predictions as shifts toward a later timing of streamflow center of mass. Discrepancies in interannual variation in spring flow patterns (as captured by DofCM) is to some degree masked in longer-term daily streamflow metrics such as NSE, percent bias, and RMSE, which are commonly used model performance metrics. These results suggest the importance of using an interannual metric such as timing of center of mass as explicit calibration and performance criteria.

[31] While the differences in snow accumulation among GRID-50, GRID-800, and 2PT-LOW are substantially less than those between 2PT-MID and MALR, the impact on

parameter selection in calibration of soil parameters is much greater. Temperature scenario 2PT-LOW produced the earliest peak snow accumulation and much earlier snowmelt relative to all other scenarios. We suggest that the relatively few and distinctive values of acceptable parameters for 2PT-LOW likely occur because of the impact of this earlier timing of snowmelt on streamflow. Similarly, MALR also calibrates for fewer acceptable parameter sets because it calculates a larger fraction of winter precipitation as snow. GRID-50, GRID-800, and 2PT-LOW tend to produce higher summer evapotranspiration (ET) losses due to a combination of earlier snowmelt, leading to an earlier start of growing-season and higher summer temperatures for 2PT-LOW and to a lesser extent GRID-50 and GRID-800 (Figure 3). Because we calibrate against the timing and magnitude of streamflow, 2PT-LOW's calibration selects for those soil moisture storage parameters that result in reduced soil moisture storage capacity relative to all other scenarios (Figures 4a and 4b). This adjustment for reduced soil moisture storage tends to reduce late summer moisture and overall basin transpiration and NPP, resulting in a greater decline of transpiration in summer growing season due to greater water stress for 2PT-LOW (Figure 8c). Calibration parameter selection and postcalibration performance show that calibration of drainage parameters can account to some extent for earlier timing of snowmelt and higher temperatures of 2PT-LOW. It is interesting to note that drainage parameter selection is more sensitive to 2PT-LOW errors that lead to earlier melt and higher summer temperatures relative to MALR errors that tend toward cold temperature and more snow. In other words, drainage parameter selection is confounded by errors in temperature estimation that are particularly evident when temperature scenarios push the system toward increased water stress.

[32] Temperature scenarios also have implications for modeling of ecologic processes. For all scenarios, mean annual model estimates of NPP and transpiration fall within a range of measured values for Pacific Northwest Douglas-fir, though GRID-800 and 2PT-MID are at the upper bounds [*Gholz*, 1982; *Granier*, 1987; *Grier et al*., 1989; *Law et al*., 2002]. There are, however, substantial differences across scenarios. Temperature estimates can influence NPP and transpiration in a variety of ways. Temperature can directly impact the rates of growing-season photosynthesis and respiration. Growing (or physiologically active) season evapotranspiration demands will also vary with each temperature scenario since VPD is calculated using temperature. Temperature also indirectly influences these fluxes by changing the timing and magnitude of growing-season water availability through changes in snow accumulation and melt. Scenarios generally show similar winter and spring fluxes, suggesting that differences in spring temperature estimates across scenarios are not a critical control. Differences in transpiration and NPP estimates across temperature scenarios occur mostly during the late summer, suggesting that differences in later summer water availability may be an important effect. There are also differences in peak transpiration and NPP values earlier in the summer, which reflect temperature controls during that period. Thus, GRID-800 has a greater plant water demand in June because it has higher temperatures at this time. Interestingly, despite receiving more precipitation as snow, MALR's growing season begins at the same time as the other temperature scenarios. MALR's maximum monthly values of NPP and transpiration are less than the minimum values for 2PT-LOW and 2PT-MID in August and September, despite MALR having two to four times the amount of snow. In other words, a larger snowpack did not result in more plant available water in the summer. It is also interesting to note the high sensitivity of 2PT-LOW's monthly transpiration and GRID-50's and GRID-800's monthly NPP to soil parameter uncertainty, demonstrating an interaction effect between errors in temperature lapse rate estimates and model sensitivity to soil parameter uncertainty. Because cross-temperature scenario differences in vegetation carbon and moisture fluxes manifest largely as a difference in late summer fluxes, we suggest that late summer VPD estimates of transpiration and temperature for NPP are important drivers, in addition to differences in water availability due to differences in soil drainage parameters. We note that it is a combination of differences in soil calibration parameters and differences in snowmelt timing that lead to differences in late summer water availability.

[33] The different temperature lapse rate scenarios also alter the sensitivity of NPP estimates to interannual variation in climate. Although GRID-800 and 2PT-MID gave similarly high values for mean annual NPP and transpiration, the 2PT-MID scenario results in higher interannual variation in these fluxes. Similarly, although both MALR and GRID-50 have the lowest NPP and transpiration estimates, MALR estimates show substantially greater interannual variation. These results demonstrate the complexity of cross-scenario differences in NPP and transpiration estimates. The lower values of mean annual MALR's NPP and transpiration suggest greater summer water stress or temperature limitations. However, this does not translate into similar sensitivity to interannual variation in climate. These differences in estimates of ecologic function, both as means and climate sensitivity, are more pronounced than differences in streamflow estimates and suggest that accurate estimates of temperature spatial patterns may be particularly important for ecohydrologic model applications designed to explore forest responses to climate change scenarios. We note that although GRID-800 and 2PT-MID produce streamflow statistics relatively close to those obtained using GRID-50, the NPP estimates from GRID-800 and 2PT-MID are substantially larger than all other scenarios. We suggest that the GRID-800 estimates of NPP, which exceed GRID-50 estimates, reflect differences in temperature estimates during the late summer. During August, GRID-800 tends to have higher NPP and lower transpiration relative to GRID-50 suggesting that GRID-800 estimates greater water use efficiency. This greater water use efficiency suggests lower temperatures and lower VPDs for a significant proportion of watershed. In general, differences among GRID-50, GRID-800, and 2PT-MID emphasize that accurate estimates of streamflow may obscure errors in estimating within watershed spatial patterns of ecosystem fluxes, and their sensitivity to climate variability.

5. Conclusion

[34] Ecohydrologic modeling provides the ability to test and refine our understanding of basin-scale relationships

between climate and the responses of hydrology and vegetation. We have shown that how we interpolate temperature in a mountain environment dominated by a rain-snow transition zone significantly influences our estimates of the timing of key hydrologic and ecosystem processes. We acknowledge that biases in other climatologic inputs, such as precipitation, can be a major source of error that influences these processes, but we focus our analysis on differences due to temperature estimation. While it is known that the mean atmospheric lapse rate typically used in hydroclimatologic modeling does not accurately represent regional conditions [*Blandford et al*., 2008; *Dobrowski et al*., 2009; *Daly et al*., 2010], an important next step is to describe how that generalization affects our understanding and model predictions in an environment where these differences in temperature representation are more likely to effect model estimates of ecohydrologic processes. Using a process-based model, this work compares a MALR to four scenarios created using two types of basin-specific temperature interpolation methods: two scenarios utilize daily-variable lapse rates created using two local meteorologic stations, and two others use spatially specific PRISM-based temperature grids. We show that given calibration, all temperature interpolation methods can be used to provide estimates of daily streamflow that yield acceptable performance measures. We note that criteria for acceptability are consistent with criteria used in other modeling studies within the western United States [*Perrin et al*., 2003; *Hay et al*., 2006]. Nonetheless, there are notable differences in seasonal streamflow behavior associated with the different temperature interpolation strategies. Model estimates of snow accumulation and melt patterns show more substantial differences that at least for two temperature strategies (2PT-LOW, MALR) are corrected for by calibration of drainage parameters. This clearly demonstrates the potential for streamflow calibration to correct for bias in temperature. Further, we note that the bias correction is much greater when that temperature scenario leads to earlier snowmelt. Calibrated parameters that correct for errors in climate input introduce bias into model projections. Because climate in the western United States is projected to warm in the future, the accuracy of model predictions regarding changes to hydrology and ecology is impacted by our interpolation of regional temperature variation.

[35] Differences in the temperature interpolation approach, even with calibration correction, lead to important differences in estimates of other ecohydrologic variables, particularly seasonal timing estimates of summer moisture stress. The temperature scenario using the MALR estimates substantially reduces later summer NPP and transpiration relative to the interpolation scenarios using regionally specific data. Scenarios also differ in the sensitivity of transpiration and NPP to interannual variation in climate drivers. These differences may have substantial impacts on future estimates of vegetation responses to warming. Though the results of this study are specific to the region, their implications present important considerations for other mountainous basins with warmer winters where the growing season is not aligned with the primary flux of precipitation inputs. Vegetation in the western United States is susceptible to water stress through the summer, and model estimates of productivity and transpiration depend on accurately representing energy demands on soil moisture. We suggest that the sensitivity of carbon sequestration to temperature estimates demonstrated by this study has implications for climate change model predictions of forests as carbon sinks.

[36] **Acknowledgments.** We thank our reviewers for the constructive feedback that greatly improved this paper. This work was supported by the funding from the USGS through the Western Mountain Initiative, the National Science Foundation (NSF) through the Willamette Watershed 2100 Project, and the UC Santa Barbara Graduate Division.

References

Ahrens, C. D. (2007), *Meteorology Today: An Introduction to Weather, Climate, and the Environment*, Thomson/Brooks/Cole, Belmont, Calif.

Bales, R. C., N. P. Molotch, T. H. Painter, M. D. Dettinger, R. Rice, and J. Dozier (2006), Mountain hydrology of the western United States, *Water Resour. Res.*, *42*, W08432, doi:10.1029/2005WR004387.

Band, L. E., C. L. Tague, P. Groffman, and K. Belt (2001), Forest ecosystem processes at the watershed scale: Hydrological and ecological controls of nitrogen export, *Hydrol. Processes*, *15*(10), 2013–2028, doi:10.1002/hyp.253.

Baron, J. S., M. D. Hartman, T. G. F. Kittel, L. E. Band, D. S. Ojima, and R. B. Lammers (1998) Effects of land cover, water redistribution, and temperature on ecosystem processes in the South Platte Basin, *Ecol. Appl.*, *8*(4), 1037–1051, doi:10.1890/1051-0761(1998)008[1037:EOLCWR]2.0.CO;2.

Barry, R. G. (1992), *Mountain Weather and Climate*, Routledge, London.

Beven, K., and J. Freer (2001), Equifinality, data assimilation, and uncertainty estimation in mechanistic modelling of complex environmental systems using the GLUE methodology, *J. Hydrol.*, *249*(1–4), 11–29, doi:10.1016/S0022–1694(01)00421-8.

Beven, K. J. (1989), Changing ideas in hydrology: The case of physically based models, *J. Hydrol.*, *105*, 157–172, doi:10.1016/0022–1694(89)90101-7.

Beven, K. J. (1996), A discussion of distributed modelling, in *Distributed Hydrological Modelling*, edited by J. C. Refsgaard and M. B. Abbott, pp. 255–278, Kluwer Acad., Norwell, Mass.

Blandford, T. R., K. S. Humes, B. J. Harshburger, B. C. Moore, V. P. Walden, and H. Ye (2008), Seasonal and synoptic variations in near-surface air temperature lapse rates in a mountainous basin, *J. Appl. Meteorol. Climatol.*, *47*(1), 249–261, doi:10.1175/2007JAMC1565.1.

Boisvenue, C., and S. W. Running (2006), Impacts of climate change on natural forest productivity—Evidence since the middle of the 20th century, *Glob. Change Biol.*, *12*(5), 862–882, doi:10.1111/j.1365–2486.2006.01134.x.

Brooks, R. H., and A. T. Corey (1964), *Hydraulic properties of porous media, Hydrol. Pap. 3*, Colo. State Univ., Fort Collins.

Cayan, D. R., S. A. Kammerdiener, M. D. Dettinger, J. M. Caprio, and D. H. Peterson (2001), Changes in the onset of spring in the western United States, *Bull. Am. Meteorol. Soc.*, *82*(3), 399–415.

Chen, J., S. C. Saunders, T. R. Crow, R. J. Naiman, K. D. Brosofske, G. D. Mroz, B. L. Brookshire, and J. F. Franklin (1999) Microclimate in forest ecosystem and landscape ecology, *BioScience*, *49*(4), 288–297.

Christensen, N. S., A. W. Wood, N. Voisin, D. P. Lettenmaier, and R. N. Palmer (2004), The effects of climate change on the hydrology and water resources of the Colorado River Basin, *Clim. Change*, *62*(1–3), 337–363, doi:10.1023/B:CLIM.0000013684.13621.1f.

Coughlan, J. C., and S. W. Running (1997), Regional ecosystem simulation: A general model for simulating snow accumulation and melt in mountainous terrain, *Landscape Ecol.*, *12*(3), 119–136, doi:10.1023/A:1007933813251.

Daly, C., and J. Smith (2005) *Mean Monthly Maximum and Minimum Air Temperature Spatial Grids (1971–2000)*, Andrews Exp. For., Long-Term Ecol. Res., For. Sci. Data Bank, Corvallis, Oreg. [Database].

Daly, C., R. P. Neilson, and D. L. Phillips (1994), A statistical-topographic model for mapping climatological precipitation over mountainous terrain, *J. Appl. Meteorol.*, *33*, 140–158, doi:10.1175/1520-0450(1994)033<0140:ASTMFM>2.0.CO;2.

Daly, C., W. P. Gibson, G. H. Taylor, G. I. Johnson, and P. Pasteris (2002), A knowledge-based approach to the statistical mapping of climate, *Clim. Res.*, *22*, 99–113, doi:10.3354/cr022099.

Daly, C., J. W. Smith, and J. I. Smith (2007), High-resolution spatial modeling of daily weather elements for a catchment in the Oregon Cascade Mountains, United States, *J. Appl. Meteorol. Climatol.*, *46*(10), 1565–1586, doi:10.1175/JAM2548.1.

Daly, C, M. Halbleib, J. I. Smith, W. P. Gibson, M. K. Doggett, G. H. Taylor, J. Curtis, and P. P. Pasteris (2008), Physiographically sensitive mapping of climatological temperature and precipitation across the conterminous United States, *Int. J. Climatol.*, *28*(15), 2031–2064, doi:10.1002/joc.1688.

Daly, C, D. R. Conklin, and M. H. Unsworth (2010), Local atmospheric decoupling in complex topography alters climate change impacts, *Int. J. Clim.*, *30*(12), 1857–1864, doi:10.1002/joc.2007.

Dingman, S. (1994), *Physical Hydrology*, Waveland Press, Inc., Long Grove, Illinois.

Dobrowski, S. Z., J. T. Abatzoglou, J. A. Greenberg, and S. G. Schladow (2009), How much influence does landscape-scale physiography have on air temperature in a mountain environment?, *Agric. For. Meteorol.*, *149*(10), 1751–1758, doi:10.1016/j.agrformet.2009.06.006.

Dodson, R., and D. Marks (1997), Daily air temperature interpolated at high spatial resolution over a large mountainous region, *Clim. Res.*, *8*(1), 1–20, doi:10.3354/cr0008001.

Franklin, J. F., and C. T. Dyrness (1988), *Natural Vegetation of Oregon and Washington*, Oreg. State Univ. Press, Corvallis.

Freer, J., McDonnell, J. J., Beven, K. J., Peters, N. E., Burns, D. A., Hooper, R. P., Aulenbach, B., and C. Kendall (2002), The role of bedrock topography on subsurface storm flow, *Water Resour. Res.*, *38*(12), 16 pp., doi:10.1029/2001WR000872.

Gerten, D., S. Schaphoff, U. Haberlandt, W. Lucht, and S. Sitch (2004), Terrestrial vegetation and water balance—Hydrological evaluation of a dynamic global vegetation model, *J. Hydrol.*, *286*(1–4), 249–270, doi:10.1016/j.jhydrol.2003.09.029.

Gholz, H. L. (1982), Environmental limits on aboveground net primary production, leaf area, and biomass in vegetation zones of the Pacific Northwest, *Ecology*, *63*, 469–481.

Granier, A. (1987), Evaluation of transpiration in a Douglas-fir stand by means of sap flow measurements, *Tree Physiol.*, *3*(4), 309–320, doi:10.1093/treephys/3.4.309.

Grier, C. C., K. M. Lee, and N. M. Nadkarni (1989), *Productivity of forests of the United States and its relation to soil and site factors and management practices: A review, Gen. Tech. Rep. PNW-GTR-222*, U.S. Dep. of Agric., For. Serv., Portland, Oreg.

Hack, J. J., J. M. Caron, S. G. Yeager, K. W. Oleson, M. M. Holland, J. E. Truesdale, and P. J. Rasch (2006), Simulation of the global hydrological cycle in the CCSM Community Atmosphere Model Version 3 (CAM3): Mean features, *J. Clim.*, *19*(11), 2199–2221, doi:10.1175/JCLI3755.1.

Hamlet, A. F., P. W. Mote, M. P. Clark, and D. P. Lettenmaier (2005), Effects of temperature and precipitation variability on snowpack trends in the western United States, *J. Clim.*, *18*, 4545–4561.

Harr, R. D. (1977), Water flux in soil and subsoil on a steep forested slope, *J. Hydrol.*, *33*(1–2), 37–58, doi:10.1016/0022–1694(77)90097-X.

Hay, L. E., and M. P. Clark (2003), Use of statistically and dynamically downscaled atmospheric model output for hydrologic simulations in three mountainous basins in the western United States, *J. Hydrol.*, *282*(1–4), 56–75, doi:10.1016/S0022–1694(03)00252-X.

Hay, L. E., G. H. Leavesley, M. P. Clark, S. L. Markstrom, R. J. Viger, and M. Umemoto (2006), Step wise, multiple objective calibration of a hydrologic model for a snowmelt dominated basin, *J. Am. Water Resour. Assoc.*, *42*(4), 877–890, doi:10.1111/j.1752-1688.2006.tb04501.x.

Huffman, G. J., R. F. Adler, M. M. Morrissey, D. T. Bolvin, S. Curtis, R. Joyce, B. McGavock, and J. Susskind (2001), Global precipitation at one-degree daily resolution from multisatellite observations, *J. Hydrometeorol.*, *2*(1), 36–50, doi:10.1175/1525–7541(2001)002<0036:GPAODD>2.0.CO;2.

Jarvis, C. H., and N. Stuart (2001), A comparison among strategies for interpolating maximum and minimum daily air temperatures. Part I: The selection of ''guiding'' topographic and land cover variables, *J. Appl. Meteorol.*, *40*(6), 1060–1074, doi:10.1175/1520-0450(2001)040<1060:ACASFI>2.0.CO;2.

Jones, H. (1992), *Plants and Microclimate: A Quantitative Approach to Plant Physiology*, Cambridge Univ. Press, Cambridge, U. K. doi:10.1086/418384.

Jung, I. and H. Chang (2011), Assessment of future runoff trends under multiple climate change scenarios in the Willamette River Basin, Oregon, USA, *Hydrol. Processes*, *25*(2), 258–277, doi:10.1002/hyp.7842.

Kirchner, J. W. (2006), Getting the right answers for the right reasons: Linking measurements, analyses, and models to advance the science of hydrology, *Water Resour. Res.*, *42*, W03S04, doi:10.1029/2005WR004362.

Law, B. E., et al. (2002), Environmental controls over carbon dioxide and water vapor exchange of terrestrial vegetation, *Agric. For. Meteorol.*, *113*(1–4), 97–120, doi:10.1016/S0168–1923(02)00104-1.

Liston, G. E., and K. Elder (2006), A meteorological distribution system for high-resolution terrestrial modeling (MicroMet), *J. Hydrometeorol.*, *7*(2), 217–234, doi:10.1175/JHM486.1.

Lookingbill, T. R., and D. L. Urban (2003), Spatial estimation of air temperature differences for landscape-scale studies in montane environments, *Agric. For. Meteorol.*, *114*(3–4), 141–151, doi:10.1016/S0168–1923(02)00196-X.

Lundquist, J. D., and D. R. Cayan (2007), Surface temperature patterns in complex terrain: Daily variations and long-term change in the central Sierra Nevada, California, *J. Geophys. Res.*, *112*, D11124, doi:10.1029/2006JD007561.

Lundquist, J. D., N. Pepin, and C. Rochford (2008), Automated algorithm for mapping regions of cold-air pooling in complex terrain. *J. Geophys. Res.*, *113*(D22107), 1–15, doi:10.1029/2008JD009879.

Lundquist, J. D., N. Pepin, and C. Rochford (2008a), Automated algorithm for mapping regions of cold-air pooling in complex terrain. *J. Geophys. Res.*, *113*, D22107, doi:10.1029/2008JD009879.

Lundquist, J. D., P. J. Newman, B. Martner, A. B. White, D. J. Gottas, and F. M. Ralph (2008b), Rain versus snow in the Sierra Nevada, California: Comparing Doppler profiling radar and surface observations of melting level, *J. Hydrometeor.*, *9*(2), 194–211, doi:10.1175/2007JHM853.1.

Luo, Y., et al. (2008), Modeled interactive effects of precipitation, temperature, and [CO_2] on ecosystem carbon and water dynamics in different climatic zones, *Glob. Change Biol.*, *14*(9), 1986–1999, doi:10.1111/j.1365–2486.2008.01629.x.

McDonnell, J. J., et al. (2007), Moving beyond heterogeneity and process complexity: A new vision for watershed hydrology, *Water Resour. Res.*, *43*, W07301, doi:10.1029/2006WR005467.

McGuire, K. J., and McDonnell, J. J. (2010), Hydrological connectivity of hillslopes and streams: Characteristic time scales and nonlinearities, *Water Resour. Res.*, *46*(10), W10543, doi:10.1029/2010WR009341.

Minder, J. R., P. W. Mote, and J. D. Lundquist (2010), Surface temperature lapse rates over complex terrain: Lessons from the Cascade Mountains, *J. Geophys. Res.*, *115*, D14122, doi:10.1029/2009JD013493.

Nash, J.E., and J.V. Sutcliffe (1970), River flow forecasting through conceptual models. Part I: A discussion of principles, *J. Hydrol.*, *10*(3), 282–290, doi:10.1016/0022–1694(70)90255-6.

Nolin, A. W., and C. Daly (2006), Mapping 'at risk' snow in the Pacific Northwest, *J. Hydrometeorol*, *7*(5), 1164–1171, doi:10.1175/JHM543.1.

Parmesan, C. (2007), Influences of species, latitudes and methodologies on estimates of phenological response to global warming, *Glob. Change Biol.*, *13*(9), 1860–1872, doi:10.1111/j.1365–2486.2007.01404.x.

Perrin, C., C. Michel, and V. Andréassian (2003), Improvement of a parsimonious model for streamflow simulation, *J. Hydrol.*, *279*(1–4), 275–289, doi:10.1016/S0022–1694(03)00225-7.

Phillips, D. L, J. Dolph, and D. Marks (1992), A comparison of geostatistical procedures for spatial analysis of precipitation in mountainous terrain, *Agric. For. Meteorol.*, *58*(1–2), 119–141, doi:10.1016/0168–1923(92)90114-J.

Pierce, D. W., T.P. Barnett, B. D. Santer, and P. J. Gleckler (2009), Selecting global climate models for regional climate change studies, *Proc. Natl. Acad. Sci.*, *106*(21), 8441–8446, doi:10.1073/pnas.0900094106.

Rothacher, J., C. Dryness, and R. Frediiksen (1967), *Hydrologic and Related Characteristics of Three Small Watersheds in the Oregon Cascades*, 54 pp., Pac. Northwest For. and Range Exp. Stn., U.S. Dep. of Agric. For. Serv. Portland, Oreg.

Running, S. W., R. R. Nemani, and R. D. Hungerford (1987), Extrapolation of synoptic meteorological data in mountainous terrain and its use for simulating forest evapotranspiration and photosynthesis, *Can. J. For. Res.*, *17*(6), 472–483, doi:10.1139/x87-081.

Ryan, M. G. (1991), Effects of climate change on plant respiration, *Ecol. Appl.*, *1*(2), 157–167, doi:10.2307/1941808.

Schwartz, M. D. (1994), Monitoring global change with phenology: The case of the spring green wave, *Int. J. Biometeorol.*, *38*(1), 18–22, doi:10.1007/BF01241799.

Schwartz, M. D, and B. E. Reiter (2000), Changes in North American spring, *Int. J. Climatol.*, *20*(8), 929–932, doi:10.1002/1097-0088(20000630)20:8<929::AID-JOC557>3.0.CO;2–5.

Seibert, J., K. Bishop, and L. Nyberg (1997), A test of TOPMODEL's ability to predict spatially distributed groundwater levels, *Hydrol. Processes*, *11*, 1131–1144, doi:10.1002/(SICI)1099-1085(199707)11:9<1131::AID-HYP549>3.3.CO;2-R.

Smith, J. W. (2002), *Mapping the thermal climate of the H. J. Andrews Experimental Forest*, Oregon, M.S. dissertation, Oreg. State Univ., Corvallis, 23 Apr. [Available at http://ir.library.oregonstate.edu/xmlui/handle/1957/9846.].

Stahl, K., R. D. Moore, J. A. Floyer, M. G. Asplin, and I. G. McKendry (2006), Comparison of approaches for spatial interpolation of daily air-temperature in a large region with complex topography and highly variable station density, *Agric. For. Meteorol.*, *139*, 224–236, doi:10.1016/j.agrformet.2006.07.004.

Stephenson, N. L., and P. J. Mantgem (2005), Forest turnover rates follow global and regional patterns of productivity, *Ecol. Lett.*, *8*(5), 524–531, doi:10.1111/j.1461-0248.2005.00746.x.

Stewart, I. T., D. R. Cayan, and M. D. Dettinger (2004), Changes in snowmelt runoff timing in western North America under a 'business as usual' climate change scenario, *Clim. Change*, *62*(1–3), 217–232, doi:10.1023/B:CLIM.0000013702.22656.e8.

Tague, C., and A. L Dugger (2010), Ecohydrology and climate change in the mountains of the western USA—A review of research and opportunities, *Geogr. Compass*, *4*(11), 1648–1663, doi:10.1111/j.1749–8198.2010.00400.x.

Tague, C., and G. E. Grant (2009), Groundwater dynamics mediate low-flow response to global warming in snow-dominated alpine regions, *Water Resour. Res.*, *45*, W07421, doi:10.1029/2008WR007179.

Tague, C., C. McMichael, A. S. Hope, J. Choate, and R. Clark (2004), Application of the RHESSys model to a California semiarid shrubland watershed, *J. Am. Water Res. Assoc.*, *40*(3), 575–589, doi:10.1111/j.1752-1688.2004.tb04444.x.

Tague, C., G. Grant, M. Farrell, J. Choate, and A. Jefferson (2008), Deep groundwater mediates streamflow response to climate warming in the Oregon Cascades, *Clim. Change*, *86*(1–2), 189–210, doi:10.1007/s10584-007-9294-8.

Tague, C. L., and L. E. Band (2004), RHESSys: Regional hydro-ecologic simulation system—An object-oriented approach to spatially distributed modeling of carbon, water, and nutrient cycling, *Earth Interact.*, *8*(19), 1–42.

U.S. Army Corps of Engineers (1956), Snow Hydrology: Summary Report of the Snow Investigations, Portland, Oreg.

VanRheenen, N. T., A. W. Wood, R. N. Palmer, and D. P. Lettenmaier (2004), Potential implications of PCM climate change scenarios for Sacramento–San Joaquin River basin hydrology and water resources, *Clim. Change*, *62*(1–3), 257–281, doi:10.1023/B:CLIM.0000013686.97342.55.

White, A. B., D. J. Gottas, E. T. Strem, F. M. Ralph, and P. J. Neiman (2002), An automated brightband height detection algorithm for use with Doppler radar spectral moments, *J. Atmos. Oceanic Technol.*, *19*(5), 687–697, doi:10.1175/1520-0426(2002)019<0687:AABHDA>2.0.CO;2.

Whiteman, C. D. (2000), *Mountain Meteorology: Fundamentals and Applications*, 355 pp., Oxford Univ. Press, Oxford.